Nonlin. Processes Geophys., 31, 247–257, 2024
https://doi.org/10.5194/npg-31-247-2024

Nonlinear Processes in Geophysics
Open Access
EGU

Evaluation of forecasts by a global data-driven weather model with and without probabilistic post-processing at Norwegian stations

John Bjørnar Bremnes, Thomas N. Nipen, and Ivar A. Seierstad

Norwegian Meteorological Institute, P.O. Box 43, Blindern, 0313 Oslo, Norway

Correspondence: John Bjørnar Bremnes (j.b.bremnes@met.no)

Received: 28 November 2023 – Discussion started: 8 December 2023
Revised: 30 April 2024 – Accepted: 6 May 2024 – Published: 25 June 2024

Abstract. During the last 2 years, tremendous progress has been made in global data-driven weather models trained on numerical weather prediction (NWP) reanalysis data. The most recent models trained on the ERA5 reanalysis at 0.25° resolution demonstrate forecast quality on par with ECMWF's high-resolution model with respect to a wide selection of verification metrics. In this study, one of these models, Pangu-Weather, is compared to several NWP models with and without probabilistic post-processing for 2 m temperature and 10 m wind speed forecasting at 183 Norwegian SYNOP (surface synoptic observation) stations up to +60 h ahead. The NWP models included are the ECMWF HRES, ECMWF ENS and the HARMONIE-AROME ensemble model MEPS with 2.5 km spatial resolution. Results show that the performances of the global models are on the same level, with Pangu-Weather being slightly better than the ECMWF models for temperature and slightly worse for wind speed. The MEPS model clearly provided the best forecasts for both parameters. The post-processing improved the forecast quality considerably for all models but to a larger extent for the coarse-resolution global models due to stronger systematic deficiencies in these. Apart from this, the main characteristics in the scores were more or less the same with and without post-processing. Our results thus confirm the conclusions from other studies that global data-driven models are promising for operational weather forecasting.

1 Introduction

Statistical machine learning methods have been applied for decades to calibrate or enhance weather forecasts based on output from numerical weather prediction (NWP) models. Since NWP models already provide very good forecasts of most quantities, simple statistical models are often sufficient for extracting predictive information in NWP model output and for making probabilistic forecasts. In contrast, recent advancements in deep learning methods have made it possible to develop more complex machine learning models based on the initial state only: first in nowcasting of precipitation (Shi et al., 2015; Ravuri et al., 2021; Leinonen et al., 2023; Zhang et al., 2023) and more recently in medium-range weather forecasting of several parameters for the entire atmosphere (Keisler, 2022; Pathak et al., 2022; Bi et al., 2023; Lam et al., 2022; Chen et al., 2023). The latter models are trained on long archives of reanalysis data with coarse spatial resolution from ERA5 (Hersbach et al., 2020, 2023) by learning one or more time steps which in an auto-regressive manner are applied to generate complete forecasts several days ahead. The training process may take days or weeks on systems with multiple graphics processing units (GPUs) or similar, but once trained predictions can be made in seconds or minutes on a single GPU. That is, only a tiny fraction of the cost of NWP-based forecasting is required for forecast generation, making these models very attractive for operational weather forecasting. The forecast accuracy of the models now seems to have reached the level of global NWP models for basic weather parameters, though not all properties of these forecasts are yet well understood. Despite this, a few weather centres are now starting to routinely produce weather forecasts using global machine learning models initiated by NWP analyses in order to explore their full potential in more detail.

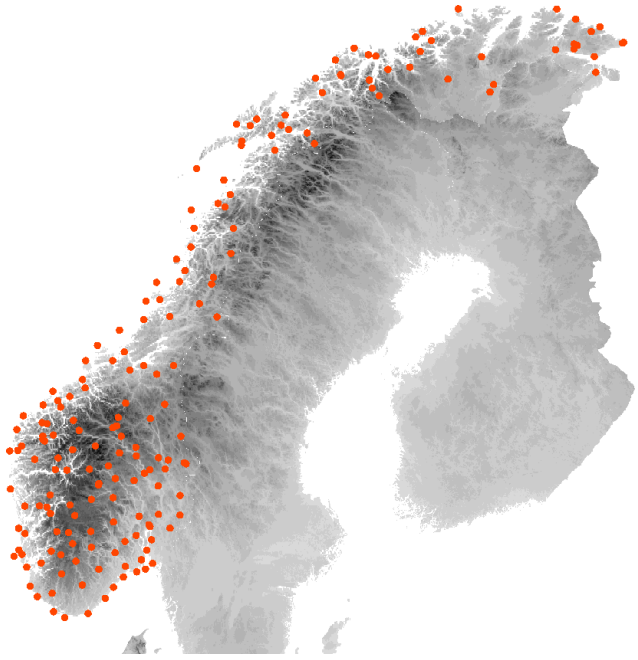

Figure 1. Location of the 183 Norwegian stations with elevation in the background. The darkest grey shade corresponds to an altitude of 2400 m.

The aim of this study is to complement the verification results already reported by the machine learning model development teams and the study of Ben-Bouallegue et al. (2023), which evaluates the performance of the Pangu-Weather model (Bi et al., 2023). The Pangu-Weather model is based on a spatial 3D transformer network with input from selected surface variables and standard upper-air variables on 13 pressure levels only. Time steps of 1, 3, 6 and 24 h are learnt and combined to generate forecasts 10 d ahead. Models for each time step are trained on 192 NVIDIA V100 GPUs for 16 d using 39 years of hourly ERA5 data. In this article, attention is paid to temperature and wind speed forecasts up to 60 h ahead, generated by the Pangu-Weather model, at a set of Norwegian SYNOP (surface synoptic observation) measurement stations. The forecasts are compared against operational forecasts from the ECMWF IFS (Integrated Forecasting System) models HRES and ENS and the HARMONIE-AROME model MEPS (Frogner et al., 2019; Andrae et al., 2020) for northern Europe at 2.5 km spatial resolution. In order to make our conclusions more robust, forecasts from all models are separately post-processed using the Bernstein quantile network method (Bremnes, 2020; Schulz and Lerch, 2022). The post-processing is capable of reducing obvious systematic deficiencies which otherwise may influence the inter-comparison.

2 Data

In order to compare the forecast models, a data set for 2 m temperature and 10 m wind speed was collected and organised for 183 Norwegian SYNOP stations for the years 2021 and 2022. The locations of the stations are shown in Fig. 1 along with the topography of Norway. The majority of the stations are situated along the coastline and fjords as well as in the valleys. Only a minority of the stations are at higher elevations. Observations with a 6-hourly temporal resolution were extracted from the Norwegian Meteorological Institute's observation database. Only stations with more than 75 % data availability during the 2-year period were included. All observations have undergone an extensive automatic quality control and to some degree a manual assessment.

Forecasts from the Pangu-Weather (PANGU) model were generated using software tools (https://github.com/ecmwf-lab/ai-models-panguweather, last access: 1 July 2023) provided by ECMWF with initial states from the ERA5 reanalysis with 0.25° spatial resolution. Further, three operational NWP models were included: ECMWF HRES available on a latitude–longitude grid of 0.1° resolution, ECMWF ENS with 51 ensemble members at 0.2° resolution and the HARMONIE-AROME model MEPS (Frogner et al., 2019; Andrae et al., 2020) for northern Europe with 15 lagged ensemble members in a 3 h time window at 2.5 km resolution. In addition, the control members of the ENS and MEPS ensembles were included in the experiments as separate deterministic models and denoted by ENS0 and MEPS0, respectively. All forecasts were initiated at 00:00 UTC with lead times +6, +12, …, +60 h and bi-linearly interpolated to the locations of the stations.

Data for the year 2021 were dedicated to training post-processing models and further split into two sets: the first 25 d in each month were used for training the models and the remaining days for selecting the best models while training as described in Sect. 4. In total there were 512 840 cases available for training, 107 515 for validation and 602 909 independent cases for comparing all models in the end. Data for the exact same times were used for all models, both for training and final evaluation.

3 Methods

In this section the probabilistic post-processing method and the verification metrics are described.

3.1 Bernstein quantile networks

There is a wide selection of post-processing methods available for making probabilistic forecasts based on either deterministic or ensemble input, e.g. Vannitsem et al. (2021). In this study, the Bernstein quantile network (BQN) (Bremnes,

2020) is chosen due to its adaptability to any continuous target variable. The key properties of the BQN are the following. First, the forecast distribution is specified by its quantile function and assumed to be a Bernstein polynomial. Second, the distribution is linked to the input variables by means of a neural network, taking any relevant set of variables as input, and outputs the coefficients of the Bernstein polynomial. The parameters of the neural network are then, in practice, the distribution parameters and can be estimated by optimising the quantile score (see below) over a pre-defined set of quantile levels. The degree of the Bernstein polynomial determines the flexibility of the distribution. By choosing a sufficiently high degree, any shape of the distribution can, in principle, be allowed for.

Let $\boldsymbol{x}$ be the vector of input variables and $\tau \in [0, 1]$ be the quantile level. The quantile function is then defined as

$$Q(\tau|\boldsymbol{x}) = \sum_{j=0}^{d} \alpha_j(\boldsymbol{x}) \binom{d}{j} \tau^j (1-\tau)^{d-j}, \tag{1}$$

where d is the degree of the Bernstein polynomial with coefficients $\alpha_j(\boldsymbol{x})$ that are functions of the input variables $\boldsymbol{x}$ or, more precisely, a neural network with input $\boldsymbol{x}$. The subsequent terms are the Bernstein basis polynomials of degree d which only depend on the quantile level τ. To ensure that the quantile function is valid, that is, non-decreasing with increasing τ, it is sufficient to constrain $\alpha_j(\boldsymbol{x})$ and $j = 0, 1, \ldots, d$ to be in non-decreasing order for any $\boldsymbol{x}$ which can be obtained by a reparameterisation of the coefficients; see Reich et al. (2011) and Schulz and Lerch (2022) for further details.

Given a training data set of input variables and observation pairs (x_i, y_i), where $i = 1, \ldots, n$, and a set of quantile levels $\tau_1, \ldots, \tau_T$, the parameters of the BQN model can be estimated by minimising

$$\sum_{i=1}^{n} \sum_{t=1}^{T} \rho_{\tau_t}(y_i - Q(\tau_t|x_i)) \tag{2}$$

with respect to the underlying parameters of $\alpha_j(\boldsymbol{x})$, that is, the weights and biases of the neural network. The quantile loss function ρ_τ is defined by

$$\rho_\tau(u) = \begin{cases} u(\tau - 1) & u < 0, \\ u\tau & u \geq 0. \end{cases} \tag{3}$$

The optimisation problem in Eq. (2) is solved numerically by stochastic gradient descent; see Sect. 4.1 for further details.

3.2 Forecast and verification metrics

In our experiments the accuracy and properties of both deterministic and probabilistic/ensemble forecasts are assessed. The metrics applied for deterministic forecasts are listed in Table 1 along with a description of how they are calculated. These include basic scores like the mean absolute error (MAE), mean error (ME) and standard deviation of error (SDE) but also measures of forecast and observed variability as well as extremes. For deterministic forecast verification, ensemble and probabilistic forecasts are reduced to their medians or 50th percentiles which are optimal with respect to absolute error.

The continuous ranked probability score (CRPS) (Matheson and Winkler, 1976; Gneiting and Raftery, 2007), which is a proper scoring function, is chosen as the summarising measure for ensemble and probabilistic forecasts. Given a single ensemble forecast of m members, $e_1, e_2, \ldots, e_m$, and a corresponding observation y, the CRPS is defined by

$$\mathrm{CRPS} = \frac{1}{m} \sum_{i=1}^{m} |e_i - y| + \frac{1}{2m^2} \sum_{i=1}^{m} \sum_{j=1}^{m} |e_i - e_j|. \tag{4}$$

The CRPS is negatively oriented; that is, lower CRPSs are preferred. In the case of only one member, the CRPS reduces to the absolute error. For several forecasts, the CRPS is just computed for each of the given forecasts and then averaged. In this study, the definition in Eq. (4) is also applied for the quantile forecasts generated by the BQN method. Further, it could be noted that, in this study, CRPSs for ensembles and sets of quantiles of different sizes are compared, which may to a minor extent, favour the largest-sized models (Ferro et al., 2008).

4 Experiments and results

In this section details on the post-processing models are first provided followed by the presentation and discussion of the results for the temperature and wind speed data sets.

4.1 Description of post-processing models

The BQN method is applied to make probabilistic forecasts of temperature and wind speed at the location of the stations using forecasts from Pangu-Weather and the NWP models as input, that is, separate BQN models for each parameter and input model. Since both deterministic (PANGU, HRES, MEPS0 and ENS0) and ensemble models (MEPS and ENS) are included in the study, different input variables to the BQN models were selected as listed in Table 2. From the input models, only the relevant forecast variable was chosen, though for wind both its magnitude and zonal and meridional components were included. For ensembles, the ensemble mean and standard deviation were used. In addition to the forecast model variables, a set of static predictors was added. Simple trigonometric functions of the day of year were applied to account for possible seasonal variations. Lead time was included for the simplicity of having one BQN model for all lead times. Variation between stations was allowed for by including the station ID as an embedding in the network

Table 1. List of verification metrics for deterministic forecasts.

Metric	Abbreviation	Description
Mean absolute error	MAE	mean absolute difference of forecasts and observations
Mean error (bias)	ME	mean difference of forecasts and observations
Standard deviation of error	SDE	standard deviation of error computed for each station and then averaged
Standard deviation ratio	SDR	standard deviation of forecasts divided by standard deviation of observations calculated for each station and then averaged
Deviation in maxima		difference between maximum forecast value and maximum observed value calculated for each station and then averaged
Deviation in minima		difference between minimum forecast value and minimum observed value calculated for each station and then averaged
Maxima ratio		maximum forecast divided by maximum observation calculated for each station and then averaged

before it was merged with the other input variables. In the embedding, each station ID was represented by eight trainable parameters in order to capture spatial variability. With 183 stations, this amounted to $183 \times 8 = 1464$ parameters in total for the embedding.

The definition of the neural network was primarily based on the studies by Bremnes (2020) and Schulz and Lerch (2022) without further hyper-parameter tuning of the data in this study. The number of fully connected/dense layers in the network was set to two with "elu" activation functions and a "softplus" transformation at the end to constrain the Bernstein coefficients to be in increasing order. The degree of the Bernstein polynomials was set to 12, which allowed for highly flexible forecast distributions. Other hyper-parameter choices and model details were as follows:

- batch size of 128 with random shuffling of the data between the epochs,
- continuous input variables standardised by subtracting means and dividing by standard deviations,
- early stopping with initial learning rate of 0.001 with a reduction by a factor of 10 if no improvement on the validation set was obtained in 10 epochs (the maximum number of epochs was set to 200, and minimum learning rate was set to 5×10^{-6}),
- ADAM optimiser with default parameters,
- quantile loss function averaged over quantile levels 0.025, 0.050, …, 0.975,
- predictions for the 0.00, 0.01, …, 1.00 quantiles.

Three network models were fitted with different numbers of units in the two dense layers: (64, 32), (32, 32) and (32, 16). In addition, each of these was trained three times with random initial parameters. All verification statistics on the test data set were averaged over these nine models to make the results more robust to model specification and random variations.

4.2 Temperature at 2 m

In Fig. 2 deterministic verification statistics for the NWP models and Pangu-Weather without any post-processing are shown as a function of lead time. With respect to MAE, MEPS (ensemble median) and MEPS0 (control member) are considerably better than the rest. The MAE for MEPS is slightly lower than for MEPS0 as expected due to the fact that the median is optimal with respect to absolute error. Further, PANGU scores better than both HRES and ENS despite being trained on coarse-resolution ERA5 data. On the other hand, it may have an advantage of being initiated with reanalysis data instead of an operational NWP analysis (Ben-Bouallegue et al., 2023). Concerning the mean error (bias), the MEPS models and PANGU have scores close to zero. The negative mean errors of HRES and ENS models are possibly due to elevation differences and a cold bias along the coast during winter (not shown). It is, however, surprising that this is not the case for PANGU. In the SDE, the mean errors are subtracted for each station before squaring the error; thus, it is invariant to possible biases. The pattern is the same as for MAE, but the differences between the models are less in percentage, in particular for the longer lead times. The SDE values for PANGU and HRES are also more similar. Forecast variation is summarised by the standard deviation ratio. HRES, ENS0 and ENS have slightly larger variation than the observations. One possible explanation may be that with a coarse model resolution, lakes and sea are not well resolved such that the sites on average are less influenced by sea/lake

Table 2. List of input variables for BQN temperature and wind speed models with deterministic and ensemble inputs. The columns for deterministic input refer to the PANGU, HRES, MEPS0 and ENS0 models, while ensemble columns refer to MEPS and ENS. Wind is represented by three variables: its magnitude and zonal and meridional components.

	Temperature		Wind speed	
Input variable	Deterministic	Ensemble	Deterministic	Ensemble
Station ID	×	×	×	×
Lead time	×	×	×	×
Cosine day of year: cos(2π d/365)	×	×	×	×
Sine day of year: sin(2π d/365)	×	×	×	×
Temperature	×			
Ensemble mean of temperature		×		
Ensemble standard deviation of temperature		×		
Wind (magnitude, zonal and meridional)			×	
Ensemble mean of wind (magnitude, zonal and meridional)			×	×
Ensemble standard deviation of wind speed			×	×

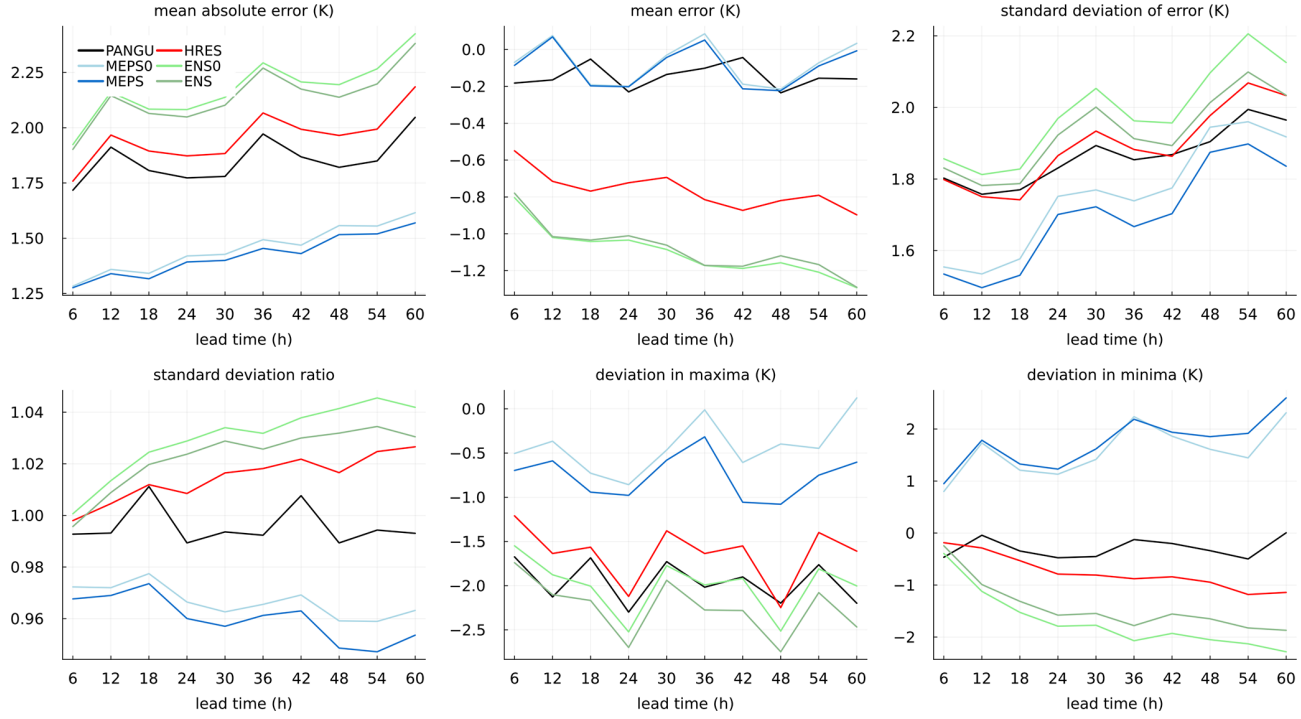

Figure 2. Deterministic forecast and verification metrics for temperature at 2 m as a function of lead time for the forecast models without post-processing.

temperatures than in reality. The average model elevation at the sites for these models are also somewhat higher than the actual elevation, although it is unknown whether this can have an impact on forecast variability. However, PANGU, which has about the same model orography as the ECMWF models, has about the same variability as the observations. Both MEPS and MEPS0 forecasts have less standard deviation than observed. Concerning temperature maxima, all models are, on average over the stations, too cold, in particular PANGU and the ECMWF models. For annual minimum temperature, the MEPS models are too warm, while the rest are too cold.

In Fig. 3 the CRPS and MAE of the medians/50th percentiles are shown for the models after post-processing as well as for the uncalibrated forecasts. From the lower panels, it can be noticed that post-processing improves the models considerably. For the ECMWF models and PANGU, the reductions are up to about 50 %, especially for ENS and ENS0. For MEPS and MEPS0, the improvements are less but still highly significant. Concerning the calibrated models, there

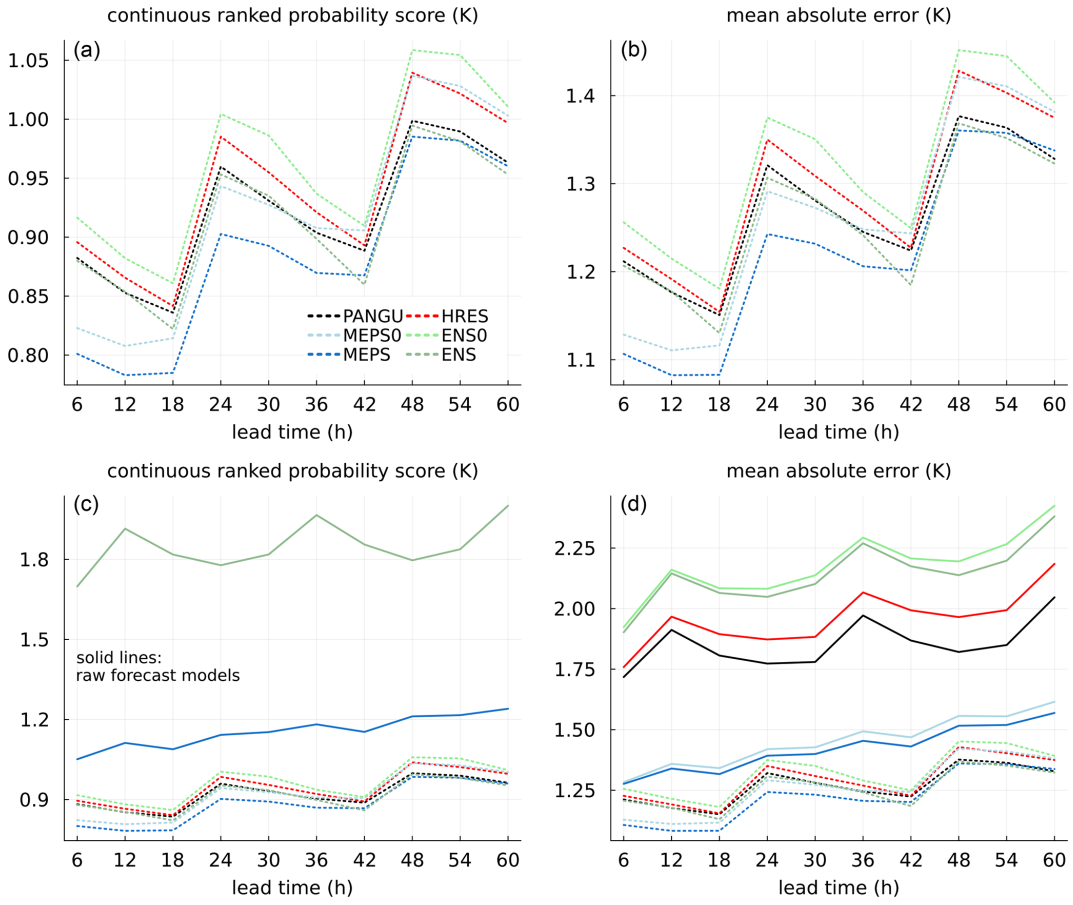

Figure 3. Continuous ranked probability score and mean absolute error for temperature at 2 m as a function of lead time. In **(a)** and **(b)** scores for BQN-calibrated forecasts only (dotted lines). In **(c)** and **(d)** raw forecast models (solid lines) are added for comparison.

is a distinct difference in skill between models with ensemble input (MEPS and ENS) and their deterministic variants using only the control members (MEPS0 and ENS0), confirming the usefulness of ensemble systems. After calibration, the difference between the models become less, in particular for longer lead times. This is due to stronger systematic errors in the models with coarser resolution which in general are easier to improve upon by post-processing methods. However, the high-resolution MEPS model still has clearly better scores than the global models, at least up to 42 h ahead. It should also be mentioned that the ECMWF models have longer data-assimilation windows than the MEPS model, making their effective lead time shorter.

To assess whether the differences in CRPS for the post-processed models are statistically significant, one-sided pairwise Diebold and Mariano (1995) hypothesis tests are applied separately for each site and lead time and the number of significant outcomes are counted; see Appendix A for more details. The testing procedure is carried out individually for all pairs of models, and the results are summarised in Table 3. As expected, PANGU and HRES have roughly equal fractions of sites and lead times where either of them is best. Further, the global models are for very few combinations (up to 16.1 %) better than MEPS, and these are likely for the longer lead times where the scores are most similar. The most significant results are for ensemble versus control member models: ENS is in 91.5 % of cases significantly better than its control member (ENS0), while MEPS is better than MEPS0 in 72.2 % of the combinations. Overall, one might have expected that the outcome of the tests would result in proportions closer to 0 % or 100 %, but it should be kept in mind that there are only up to 365 forecast cases in each pairwise test. With a nominal significance level of 0.05, the differences are often too small to be of statistical significance with the current data size. An alternative would be to apply the testing procedure separately for each lead time. For the shorter lead times, it is reasonable to anticipate stronger significance results for MEPS for instance.

4.3 Wind speed at 10 m

Deterministic verification metrics for the 10 m wind speed forecasts without post-processing are presented in Fig. 4. As expected, MEPS and MEPS0 are clearly better than HRES,

Table 3. Proportion (%) of site and lead time combinations (183 × 10 in total) where the model in a given row is statistically significantly better than those in the columns with respect to CRPS. The results are for post-processed 2 m temperature forecasts.

	PANGU	HRES	ENS	MEPS	ENS0	MEPS0
PANGU		33.6	28.4	14.4	42.5	20.3
HRES	27.9		23.7	9.3	44.3	17.6
ENS	39.1	46.1		16.1	91.5	26.1
MEPS	45.5	49.2	40.1		53.6	72.2
ENS0	20.9	23.1	1.6	6.3		11.9
MEPS0	28.9	32.2	24.8	3.6	36.3	

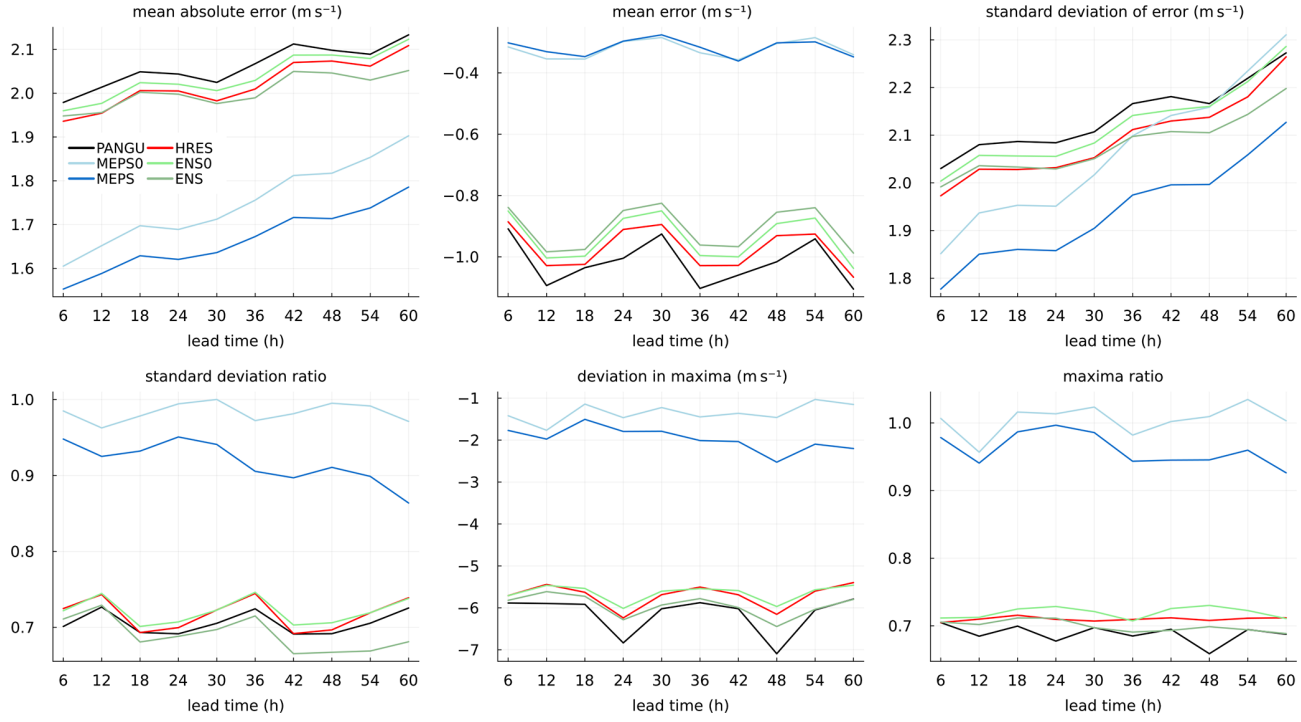

Figure 4. Forecast and verification metrics for wind speed at 10 m as a function of lead time for the forecast models without post-processing.

ENS, ENS0 and PANGU with respect to MAE. Unlike temperature, the ECMWF models have slightly better scores than PANGU for all lead times. The differences in MAE between the ECMWF models and the MEPS models are partly due to the relatively large systematic underestimation of wind speed for the ECMWF models as shown in the mean error panel. A negative bias can be noticed for all models but in particular for HRES, ENS, ENS0 and PANGU. The standard deviation of error reveals the same pattern as for MAE with the largest differences for short lead times. That is, with decreasing predictability the differences become less clear. For longer lead times, high-resolution NWP models are more prone to displacement errors in time and space than models with smoother forecast fields. This may have an impact on verification against point measurements as here. The forecast variability of HRES, ENS, ENS0 and PANGU are only about 70 % of the observed variability as quantified by the standard deviation ratio. These models also severely underestimate extreme wind speeds. Averaged over the stations, the annual forecast wind speed maxima are about 6 m s^{-1} weaker than the observed maxima. The panel showing the maxima ratio also confirms this. For MEPS, the model climatology is much closer to the observed. For the control member (MEPS0), the standard deviation and maxima ratios are close to one, while there is an underestimation of about 1.5 m s^{-1} of the annual extremes. The MEPS (ensemble median) has less variability than MEPS0 as expected by construction.

CRPS and MAE for the post-processed probabilistic forecasts and the raw models are shown in Fig. 5. In the lower panels the benefits of post-processing are evident. For example, for ENS the CRPS is reduced by up to about 50 % and for MEPS about 35 %. This can partly be attributed to BQN models being capable of learning local systematic deviations. For wind speed, there may be strong fine-scale vari-

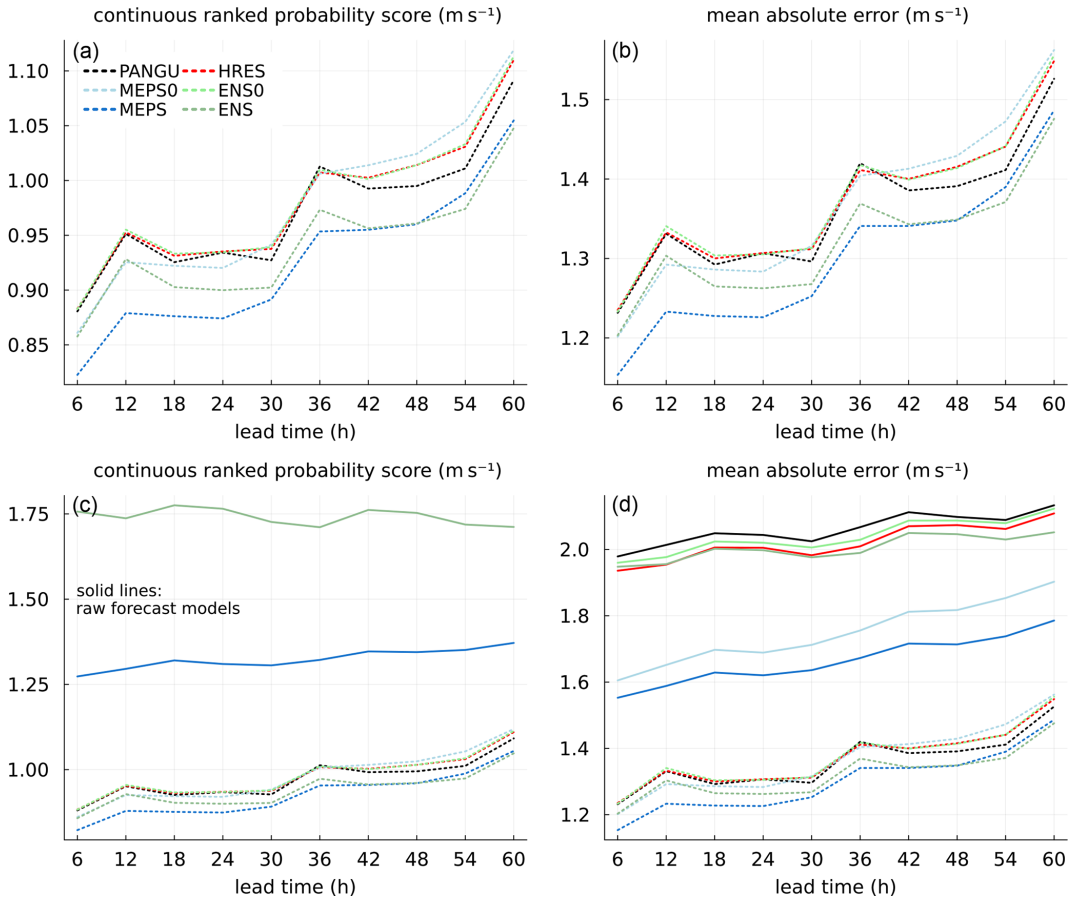

Figure 5. Continuous ranked probability score and mean absolute error for wind speed at 10 m as a function of lead time. In **(a)** and **(b)** scores are for BQN-calibrated forecasts only (dotted lines). **(c)** and **(d)** are also including raw forecast models (solid lines).

ability in the proximity of most stations that NWP models are not able to represent. Further, models based on ensemble input are consistently better than deterministic ones, thus again confirming the usefulness of ensemble forecast systems. For the longer lead times, Pangu-Weather seems to benefit more from post-processing than the ECMWF models, which could be due to smoother forecast fields, but this needs further investigation.

As for temperature, testing statistical significance of differences in CRPS was performed for the post-processed wind speed forecasts in a pairwise manner. The proportions of site and lead time combinations where each model is better than the remaining models are given in Table 4. The difference between PANGU and HRES is clearly negligible. MEPS is significantly better than the global models for roughly half of the 183×10 site and lead time combinations, which is mostly due to the differences for the shorter lead times.

5 Conclusions

In this study, we have compared the forecast accuracy of the Pangu-Weather model with global NWP models from ECMWF and the high-resolution limited-area model MEPS by verifying against Norwegian SYNOP measurements. In addition, probabilistic post-processed forecasts from all ensemble and deterministic models have been evaluated. The latter models are especially useful for better showing the full potential in each of the models as they are capable of removing systematic deviations. Besides, in many forecast products for end users, post-processing is frequently applied, making our comparisons even more relevant. In this sense, our study has complemented the assessments of Bi et al. (2023) and Ben-Bouallegue et al. (2023).

The main finding of our work is that Pangu-Weather is slightly better than the ECMWF models for temperature and vice versa for wind speed. For temperature, the differences are mostly due to less bias in Pangu-Weather, while for wind speed differences in bias are less obvious. The global models are, however, considerably less skilful than the high-resolution MEPS model. After post-processing, the differences decrease significantly due to larger systematic errors in the coarse-scale Pangu-Weather and ECMWF models, which post-processing methods can effectively remove. For the longer lead times, the summarising scores are highly

Table 4. Proportion (%) of site and lead time combinations (183×10 in total) where the model in a given row is statistically significantly better than those in the columns with respect to CRPS. The results are for post-processed 10m wind speed forecasts.

	PANGU	HRES	ENS	MEPS	ENS0	MEPS0
PANGU		27.5	15.2	7.0	32.8	20.6
HRES	28.9		18.1	9.2	36.6	24.9
ENS	50.4	54.5		19.3	91.6	40.5
MEPS	54.8	52.1	42.3		56.4	88.2
ENS0	27.7	31.0	2.8	8.3		23.6
MEPS0	23.9	24.4	15.9	0.5	27.5	

similar. Our study also clearly shows the advantage of NWP ensemble forecasting.

There is certainly scope for further work. A more in-depth evaluation at station and seasonal levels would be needed to discover more of the characteristics of Pangu-Weather and global data-driven machine learning models in general. Another and much debated topic, which we have not looked into, is the amount of space–time smoothing with increasing lead time. Regarding post-processing methods, it would be useful to set up experiments with more predictor variables (or even different methods) and study their impacts. Further, with post-processing it would be interesting to evaluate predictions beyond point measurements; for example, gridded products or space–time functionals like the maximum wind speed over a larger area during a 12 h period, say, would be instructive. If other high-impact variables like precipitation become available, then these would be of interest for an intercomparison. The same would apply to forecast products tailored to specific end users, for example within the energy sector. Since the Pangu-Weather model was published, further improvements in global machine learning models have been made (Lam et al., 2022; Chen et al., 2023). A follow-up study with post-processing of several machine learning models would be interesting as well as ensembles generated by purely data-driven machine learning models. Finally, there is ongoing work on training global graph-based machine learning models with kilometre-scale resolution over regions of special interest and coarser resolution elsewhere. These models make use of long archives of high-resolution limited-area reanalysis data in combination with global reanalyses like ERA5. Comparing these with limited-area NWP models like MEPS will be of great interest.

Appendix A: Testing statistical significance

Testing statistical significance is challenging due to complex dependencies in space and time, and there are several ways forward. Hence, it is important to be aware that the outcome would depend on how such tests are set up and the purpose. We have chosen to focus on site- and lead-time-specific performance by applying the Diebold and Mariano (1995) test separately for each site and lead time and using the Benjamini and Hochberg (1995) procedure to control the false discovery rate at the given nominal level. Before the testing procedure is applied, each forecast model is averaged over its 3×3 variants of initial states and network configurations; see Sect. 4.1. The testing procedure is here only applied to the post-processed forecasts. The proportion of the 183×10 site and lead time combinations where a given model is significantly better than the alternative model at the 0.05 nominal level is reported. This is the same procedure that was applied by Schulz and Lerch (2022) and suggested by Wilks (2016). We refer to those references for further mathematical details.

Code and data availability. The methods and analyses are implemented in Julia and based on the Flux package for machine learning (Innes et al., 2018; Innes, 2018). Source codes are made available on GitHub at https://doi.org/10.5281/zenodo.12204908 (Bremnes, 2024). The data (about 3 GB) can be downloaded from https://doi.org/10.5281/zenodo.10210203 (Bremnes, 2023).

Author contributions. JBB prepared the NWP and observational data, generated the post-processed forecasts, computed the verification statistics, and prepared the manuscript. TNN generated the Pangu-Weather forecasts. TNN and IAS contributed to the analysis of the results and to finalising the article.

Competing interests. The contact author has declared that none of the authors has any competing interests.

Disclaimer. Publisher's note: Copernicus Publications remains neutral with regard to jurisdictional claims made in the text, published maps, institutional affiliations, or any other geographical representation in this paper. While Copernicus Publications makes every effort to include appropriate place names, the final responsibility lies with the authors.

Acknowledgements. We would like to acknowledge Huawei Cloud for making the trained Pangu-Weather model available, ECMWF for the software to generate Pangu-Weather forecasts, and

Jørn Kristiansen and two anonymous reviewers for their feedback on the manuscript.

Review statement. This paper was edited by Zoltan Toth and reviewed by two anonymous referees.

References

Andrae, U., Frogner, I.-L., and Vignes, O.: A continuous EDA based ensemble in MetCoOp, Tech. Rep. 14, ALADIN-HIRLAM Newsletter, 2020.

Ben-Bouallegue, Z., Clare, M. C. A., Magnusson, L., Gascon, E., Maier-Gerber, M., Janousek, M., Rodwell, M., Pinault, F., Dramsch, J. S., Lang, S. T. K., Raoult, B., Rabier, F., Chevallier, M., Sandu, I., Dueben, P., Chantry, M., and Pappenberger, F.: The rise of data-driven weather forecasting, arXiv [preprint], https://doi.org/10.48550/arXiv.2307.10128, 2023.

Benjamini, Y. and Hochberg, Y.: Controlling the False Discovery Rate: A Practical and Powerful Approach to Multiple Testing, J. Roy. Stat. Soc. B, 57, 289–300, 1995.

Bi, K., Xie, L., Zhang, H., Chen, X., Gu, X., and Tao, Q.: Accurate medium-range global weather forecasting with 3D neural networks, Nature, 619, 533–538, https://doi.org/10.1038/s41586-023-06185-3, 2023.

Bremnes, J. B.: Ensemble Postprocessing Using Quantile Function Regression Based on Neural Networks and Bernstein Polynomials, Mon. Weather Rev., 148, 403–414, https://doi.org/10.1175/MWR-D-19-0227.1, 2020.

Bremnes, J. B.: Weather forecasts from multiple models and observations at Norwegian synop stations, Zenodo [data set], https://doi.org/10.5281/zenodo.10210203, 2023.

Bremnes, J. B.: Source code: Evaluation of forecasts by a global data-driven weather model with and without probabilistic post-processing at Norwegian stations. In Nonlinear Processes in Geophysics (v0.1.1), Zenodo [code], https://doi.org/10.5281/zenodo.12204908, 2024.

Chen, K., Han, T., Junchao, G., Lei, B., Fenghua, L., Luo, J.-J., Chen, X., Ma, L., Zhang, T., Su, R., Ci, Y., Li, B., Yang, X., and Ouyang, W.: FengWu: Pushing the Skillful Global Medium-range Weather Forecast beyond 10 Days Lead, arXiv [preprint], https://doi.org/10.48550/arXiv.2304.02948, 2023.

Diebold, F. and Mariano, R.: Comparing Predictive Accuracy, J. Bus. Econ. Stat., 13, 253–63, 1995.

Ferro, C. A. T., Richardson, D. S., and Weigel, A. P.: On the effect of ensemble size on the discrete and continuous ranked probability scores, Meteorol. Appl., 15, 19–24, https://doi.org/10.1002/met.45, 2008.

Frogner, I.-L., Andrae, U., Bojarova, J., Callado, A., Escribà, P., Feddersen, H., Hally, A., Kauhanen, J., Randriamampianina, R., Singleton, A., Smet, G., van der Veen, S., and Vignes, O.: HarmonEPS – The HARMONIE Ensemble Prediction System, Weather Forecast., 34, 1909–1937, https://doi.org/10.1175/WAF-D-19-0030.1, 2019.

Gneiting, T. and Raftery, A. E.: Strictly proper scoring rules, prediction, and estimation, J. Am. Stat. A., 102, 359–378, https://doi.org/10.1198/016214506000001437, 2007.

Hersbach, H., Bell, B., Berrisford, P., Hirahara, S., Horányi, A., Muñoz-Sabater, J., Nicolas, J., Peubey, C., Radu, R., Schepers, D., Simmons, A., Soci, C., Abdalla, S., Abellan, X., Balsamo, G., Bechtold, P., Biavati, G., Bidlot, J., Bonavita, M., De Chiara, G., Dahlgren, P., Dee, D., Diamantakis, M., Dragani, R., Flemming, J., Forbes, R., Fuentes, M., Geer, A., Haimberger, L., Healy, S., Hogan, R. J., Hólm, E., Janisková, M., Keeley, S., Laloyaux, P., Lopez, P., Lupu, C., Radnoti, G., de Rosnay, P., Rozum, I., Vamborg, F., Villaume, S., and Thépaut, J.-N.: The ERA5 global reanalysis, Q. J. Roy. Meteor. Soc., 146, 1999–2049, https://doi.org/10.1002/qj.3803, 2020.

Hersbach, H., Bell, B., Berrisford, P., Biavati, G., Horányi, A., Muñoz Sabater, J., Nicolas, J., Peubey, C., Radu, R., Rozum, I., Schepers, D., Simmons, A., Soci, C., Dee, D., and Thépaut, J.-N.: ERA5 hourly data on single levels from 1940 to present, Copernicus Climate Change Service (C3S) Climate Data Store (CDS) [data set], https://doi.org/10.24381/cds.adbb2d47, 2023.

Innes, M.: Flux: Elegant Machine Learning with Julia, J. Open Source Softw., 3, 602, https://doi.org/10.21105/joss.00602, 2018.

Innes, M., Saba, E., Fischer, K., Gandhi, D., Rudilosso, M. C., Joy, N. M., Karmali, T., Pal, A., and Shah, V.: Fashionable Modelling with Flux, CoRR, abs/1811.01457, arxiv [preprint], https://doi.org/10.48550/arXiv.1811.01457, 2018.

Keisler, R.: Forecasting Global Weather with Graph Neural Networks, arXiv [preprint], https://doi.org/10.48550/arXiv.2202.07575, 2022.

Lam, R., Sanchez-Gonzalez, A., Willson, M., Wirnsberger, P., Fortunato, M., Pritzel, A., Ravuri, S., Ewalds, T., Alet, F., Eaton-Rosen, Z., Hu, W., Merose, A., Hoyer, S., Holland, G., Stott, J., Vinyals, O., Mohamed, S., and Battaglia, P.: GraphCast: Learning skillful medium-range global weather forecasting, arXiv [preprint], https://doi.org/10.48550/arXiv.2212.12794, 2022.

Leinonen, J., Hamann, U., Nerini, D., Germann, U., and Franch, G.: Latent diffusion models for generative precipitation nowcasting with accurate uncertainty quantification, arXiv [preprint], https://doi.org/10.48550/arXiv.2304.12891, 2023.

Matheson, J. E. and Winkler, R. L.: Scoring Rules for Continuous Probability Distributions, Management Science, 22, 1087–1096, 1976.

Pathak, J., Subramanian, S., Harrington, P., Raja, S., Chattopadhyay, A., Mardani, M., Kurth, T., Hall, D., Li, Z., Azizzadenesheli, K., Hassanzadeh, P., Kashinath, K., and Anandkumar, A.: FourCastNet: A Global Data-driven High-resolution Weather Model using Adaptive Fourier Neural Operators, arXiv [preprint], https://doi.org/10.48550/arXiv.2202.11214, 2022.

Ravuri, S., Lenc, K., Willson, M., Kangin, D., Lam, R., Mirowski, P., Fitzsimons, M., Athanassiadou, M., Kashem, S., Madge, S., Prudden, R., Mandhane, A., Clark, A., Brock, A., Simonyan, K., Hadsell, R., Robinson, N., Clancy, E., Arribas, A., and Mohamed, S.: Skilful precipitation nowcasting using deep generative models of radar, Nature, 597, 672–677, https://doi.org/10.1038/s41586-021-03854-z, 2021.

Reich, B. J., Fuentes, M., and Dunson, D. B.: Bayesian Spatial Quantile Regression, J. Am. Stat. A., 106, 6–20, https://doi.org/10.1198/jasa.2010.ap09237, 2011.

Schulz, B. and Lerch, S.: Machine Learning Methods for Postprocessing Ensemble Forecasts of Wind Gusts: A Sys-

tematic Comparison, Mon. Weather Rev., 150, 235–257, https://doi.org/10.1175/MWR-D-21-0150.1, 2022.

Shi, X., Chen, Z., Wang, H., Yeung, D.-Y., Wong, W.-k., and Woo, W.-c.: Convolutional LSTM Network: A Machine Learning Approach for Precipitation Nowcasting, in: Proceedings of the 28th International Conference on Neural Information Processing Systems – Volume 1, NIPS'15, 802–810, MIT Press, Cambridge, MA, USA, 2015.

Vannitsem, S., Bremnes, J. B., Demaeyer, J., Evans, G. R., Flowerdew, J., Hemri, S., Lerch, S., Roberts, N., Theis, S., Atencia, A., Bouallègue, Z. B., Bhend, J., Dabernig, M., Cruz, L. D., Hieta, L., Mestre, O., Moret, L., Plenković, I. O., Schmeits, M., Taillardat, M., den Bergh, J. V., Schaeybroeck, B. V., Whan, K., and Ylhaisi, J.: Statistical Postprocessing for Weather Forecasts: Review, Challenges, and Avenues in a Big Data World, B. Am. Meteorol. Soc., 102, E681–E699, https://doi.org/10.1175/BAMS-D-19-0308.1, 2021.

Wilks, D. S.: "The stippling shows statistically significant grid points": How research results are routinely overstated and overinterpreted, and what to do about it, B. Am. Meteorol. Soc., 97, 2263–2273, 2016.

Zhang, Y., Long, M., Chen, K., Xing, L., Jin, R., and Jordan, M. I.: Skilful nowcasting of extreme precipitation with NowcastNet, Nature, 619, 526–532, https://doi.org/10.1038/s41586-023-06184-4, 2023.